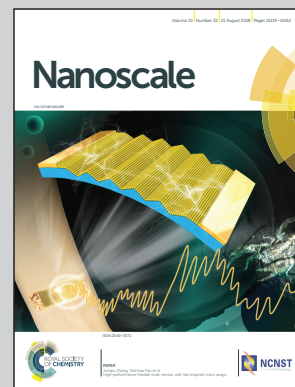


Showcasing research from the Department of Physics,
Tsinghua University, Beijing, China.

Flexible, transparent and highly sensitive SERS substrates with
cross-nanoporous structures for fast on-site detection

A flexible and transparent SERS substrate with a large number of metal nanogaps and sharp edges is fabricated on PET film via a cost-effective strategy. The strong signal enhancement can be excited under the irradiation of an incident laser. Using the flexible substrate as a SERS platform, the fast, on-site and ultrasensitive SERS detection of contaminants and pesticides remaining on the skins of fruits is realized through wrapping and swabbing techniques. These versatile substrates are promising for practical application in rapid, on-site SERS-based detection.

As featured in:



See Qunqing Li et al., *Nanoscale*,
2018, 10, 15195.




rsc.li/nanoscale

Registered charity number: 207890



Cite this: *Nanoscale*, 2018, **10**, 15195

Flexible, transparent and highly sensitive SERS substrates with cross-nanoporous structures for fast on-site detection†

Yingcheng Wang,^{a,b} Yuanhao Jin,^{a,b} Xiaoyang Xiao,^{a,b} Tianfu Zhang,^{a,b} Haitao Yang,^{a,b} Yudan Zhao,^{a,b} Jiaping Wang,^{a,b} Kaili Jiang,^{a,b} Shoushan Fan^{a,b} and Qunqing Li  ^{a,b}

A flexible and transparent film assembled from the cross-nanoporous structures of Au on PET (CNS of Au@PET) is developed as a versatile and effective SERS substrate for rapid, on-site trace analysis with high sensitivity. The fabrication of the CNS of Au can be achieved on a large scale at low cost by employing an etching process with super-aligned carbon nanotubes as a mask, followed by metal deposition. A strongly enhanced Raman signal with good uniformity can be obtained, which is attributed to the excitation of “hot spots” around the metal nanogaps and sharp edges. Using the CNS of Au@PET film as a SERS platform, real-time and on-site SERS detection of the food contaminant crystal violet (CV) is achieved, with a detection limit of CV solution on a tomato skin of 10^{-7} M. Owing to its ability to efficiently extract trace analytes, the resulting substrate also achieves detection of 4-ATP contaminants and thiram pesticides by swabbing the skin of an apple. A SERS detection signal for 4-ATP has a relative standard deviation of less than 10%, revealing the excellent reproducibility of the substrate. The flexible, transparent and highly sensitive substrates fabricated using this simple and cost-effective strategy are promising for practical application in rapid, on-site SERS-based detection.

Received 27th February 2018,
Accepted 8th May 2018

DOI: 10.1039/c8nr01628c

rsc.li/nanoscale

Introduction

Surface-enhanced Raman Scattering (SERS),^{1,2} one of the most powerful sensing techniques for identifying molecule vibrational spectra with high sensitivity and selectivity, has attracted worldwide research interest in recent years.^{3–5} Owing to its high performance and nondestructive characteristics,^{6,7} SERS technology provides a robust method for the trace level detection of analytes,^{8,9} and is extensively applied in the fields of environmental monitoring,¹⁰ explosives detection,¹¹ homeland security,¹² and biomedical science.^{13,14}

The main mechanisms of SERS activity are attributed to the large local electromagnetic (EM) field enhancement and chemical enhancement.^{2,15,16} The EM mechanism can make a dominant contribution by a factor of 10^4 – 10^{10} to the Raman signal enhancement.^{8,17,18} It is widely believed that the large EM field enhancement is supported by the optical excitation of localized surface plasmon resonance (LSPR), termed field “hot spots”, in the vicinity of metallic nanostructures, especially around the narrow nanogaps and sharp edges.^{19,20} As a result, considerable effort in the development of SERS-active substrates, has been aimed at designing and optimizing the geometry, dimensions and arrangement of metallic nanostructures, to generate a high density of “hot spots”.^{18,21,22} Two approaches are primarily used for the fabrication of SERS substrates: top-down and bottom-up.²³ The former is based on standard lithography such as electron-beam lithography (EBL) and nanoimprint lithography.^{20,24,25} Despite the pronounced and stable SERS signals that can be obtained from the plasmonic nanostructures prepared using these methods,²⁶ simplicity, low cost and high throughput are compromised. The latter involves colloidal self-assembly and electrochemical reduction of noble metal salts, which inevitably results in limited reproducibility.^{27,28} In addition, these supporting substrates are often based on rigid templates (such as silicon and quartz), which limits their utility in real-world applications owing to their brittle nature.²⁹

^aState Key Laboratory of Low-Dimensional Quantum Physics, Department of Physics & Tsinghua-Foxconn Nanotechnology Research Center, Tsinghua University, Beijing 100084, China. E-mail: qunqli@mail.tsinghua.edu.cn

^bCollaborative Innovation Center of Quantum Matter, Beijing, China

†Electronic supplementary information (ESI) available: Preparation and characterization of pure SACNT films, morphology characterization and finite difference time domain (FDTD) simulation of 10 nm Au@PET, cross-nanoporous model and results of FDTD simulations, effect of mechanical bending on the SERS performance of flexible substrates, vibrational assignments of Raman bands in SERS spectra for different analytes, SERS detection of thiram pesticides using the flexible SERS substrate with a swabbing technique, and the intensity distribution of several vibrational bands of 4-ATP with a corresponding calculated RSD.

In contrast, flexible SERS substrates are a promising alternative for routine application because of their flexibility and transparency, in combination with high sensitivity.³⁰ In particular, they can collect trace amounts of sample from irregular surfaces such as cloth and curved glass by easy and efficient physical swabbing,^{30–32} compared with conventional hard SERS substrates. More importantly, it has been demonstrated that transparent and flexible SERS substrates are suitable for real-time, fast, *in situ* SERS detection of analytes;^{29,33} such as on-site measurement of residual contaminants on fish skin,²⁷ or real-time molecule analysis *via* a flexible SERS substrate floating on a liquid surface.³⁴ In addition, compatibility with flexible photonic and electronic devices, and the ability to be used cooperatively with portable Raman spectrometers, are also regarded as advantages of flexible SERS substrates for real-world application.^{29,35} To date, significant attention has been paid to the fabrication of flexible SERS-active substrates using tapes,³⁶ thermoplastic materials,³⁷ and polymer films^{38,39} as support materials. However, as a consumable product for molecule detection in practical applications, the ideal flexible SERS-active substrate should demonstrate high sensitivity, excellent adaptability, and good uniformity as well as being cost-effective. The tradeoff between these features results in some challenges when developing SERS-active substrates.

In this work, we present and demonstrate a simple and low cost fabrication strategy, using etching and metal evaporation, for the manufacture of versatile plasmonic SERS substrates, based on cross stacking super-aligned carbon nanotube (SACNT) films. Cross-nanoporous structures of Au, with large numbers of nanogaps and sharp edges, which can serve as “hot spots” during SERS detection, are fabricated on polyethylene terephthalate (PET) supports. Thus, the resultant SERS substrates with nanostructured SACNT features are flexible and transparent, while still possessing high activity. This makes them appropriate for real-time and on-site SERS detection of biological and chemical molecules on irregular objects.

The food contaminant crystal violet (CV) was detected at different concentrations on the surface of tomatoes and the SERS detection of 4-aminothiophenol (4-ATP) and thiram using the flexible SERS substrate with a swabbing technique was also systematically investigated. Furthermore, a low relative standard deviation (RSD) of less than 10% of the 4-ATP SERS signals was achieved, which reveals the high reproducibility of the flexible SERS substrate. The flexible SERS substrate with cross-nanoporous structures could be easily produced on a large scale using the reported approach. This cost-effective fabrication method will make the resulting flexible substrate an outstanding platform for fast, on-site SERS detection in routine applications.

Results and discussion

The steps for the fabrication of the flexible, transparent SERS substrate are outlined in Fig. 1. It has been the aim of our group to gain an understanding of the characteristics of nanostructured arrays of SACNT networks, and some applications have been explored.⁴⁰ In previous work, we established highly sensitive SERS substrates on silicon supports with good reproducibility, using a similar fabrication approach. These substrates were then applied to the detection of residues of the pesticide phosmet, with ultralow concentrations.⁴¹ Here we expand this method to flexible substrates such as plastic PET. Specifically, SiO₂ with a thickness of 500 nm was preferentially grown on PET by low temperature plasma-enhanced chemical vapor deposition (PECVD). The pure SACNT films were continuously drawn from super-aligned carbon nanotube arrays and easily cross-stacked on a metal frame by suspension (see details in ESI Fig. S1†),^{42,43} forming SACNT networks with nanoporous structures. The resulting SACNT networks were then transferred onto a ready-made SiO₂/PET substrate with the assistance of alcohol, as described in the Experimental section. This method is applicable to other substrates with low

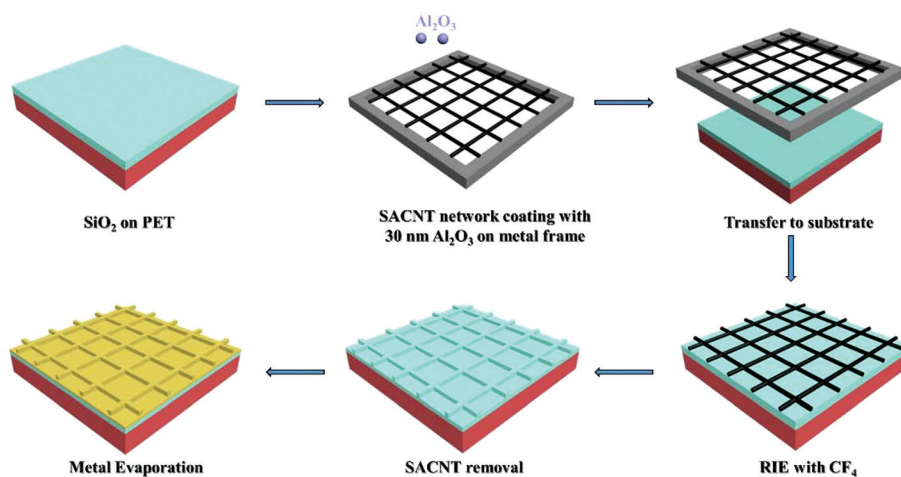


Fig. 1 Schematic of the fabrication of a flexible and transparent SERS substrate based on cross stacking SACNT films *via* etching and metal deposition.

surface roughness. Subsequently, cross-nanoporous structures (CNS) of SiO_2 were fabricated using SACNT networks as etching masks. According to our previous simulations and analysis,⁴² to obtain significant Raman enhancement, CNS of SiO_2 with an optimal depth of 200–250 nm should be pursued, which can be attained by adjusting the parameters of the reactive ion etching (RIE) process. The SACNT networks were completely removed using acetone under ultrasonication for several minutes. Finally, gold nanoparticles, with a critical thickness of 10 nm, were formed as the SERS-active layer on the cross-nanoporous surface by e-beam evaporation. This generated abundant “hot spots”, which significantly enhanced the plasmonic electromagnetic field and accounted for the large SERS enhancement in the presence of analytes discussed below.

SACNT networks with crossed arrangements can be prepared in large quantities owing to the possibility of batch growth of SACNT arrays.⁴³ A representative SEM view of crossed stacked SACNT networks is shown in Fig. S1,[†] demonstrating a quasi-periodic pattern in both the x and y directions with innumerable nanopores. Thus, mass production of flexible SERS substrates using the above procedures is cost-effective. However, the naked SACNT networks are not sufficiently durable when used as masks during the etching process. As a result, prior to the transfer process, a more robust aluminum oxide layer, with a thickness of 30 nm was deposited on the suspended SACNT films by e-beam evaporation, which can clearly strengthen their endurance. According to our previous study,^{41,42} the carbon nanotubes in cross-stacking SACNT films show complete Al_2O_3 coverage, meaning that the composite system could play an effective role as an etching

mask in the subsequent reactive ion etching of the SiO_2 located underneath. In this way, it would be possible to replicate the key features of nanostructured SACNT films in a variety of systems, by choosing an appropriate metal oxide coating and tuning the etching parameters. Further applications of these SACNT films will be explored based on this fabrication process.

In the above procedure, it is crucial to transfer the suspended SACNT networks onto the intended substrate, while maintaining their nanoporous structures. Fig. 2(a) shows the detailed morphology of the SACNT networks coated with a 30 nm Al_2O_3 layer, which was placed on a ready-made SiO_2 /PET substrate. It can be seen that the CNTs in the SACNT films are unidirectional, aligned in a parallel manner, and form a robust CNT grid when two layers are cross-stacked, so as to ensure the adequate utilization of the nanoporous structures of the as-prepared SACNT frameworks during the following RIE process. The inset shows the image with higher magnification. After RIE processing and removal of residual SACNTs, the most pronounced features of the quasi-periodic SACNT films were fully transferred to the surface of the 500 nm thick SiO_2 layer deposited on the PET. This resulted in CNS of SiO_2 , as the optical microscopy image in Fig. 2(b) shows. Given that the final electromagnetic SERS enhancement factor has a strong correlation with the aspect ratio of the nanostructured array,⁷ we carefully tuned the etching conditions of the carbon tetrafluoride (CF_4) plasma, including radio-frequency (RF) power and etching time. The SiO_2 etching conditions were 40 sccm (standard-state cubic centimeters per minute), a CF_4 pressure of 4 Pa and a RF power of 50 W. The operating time was optimized to 6 minutes to obtain a nanostructured depth

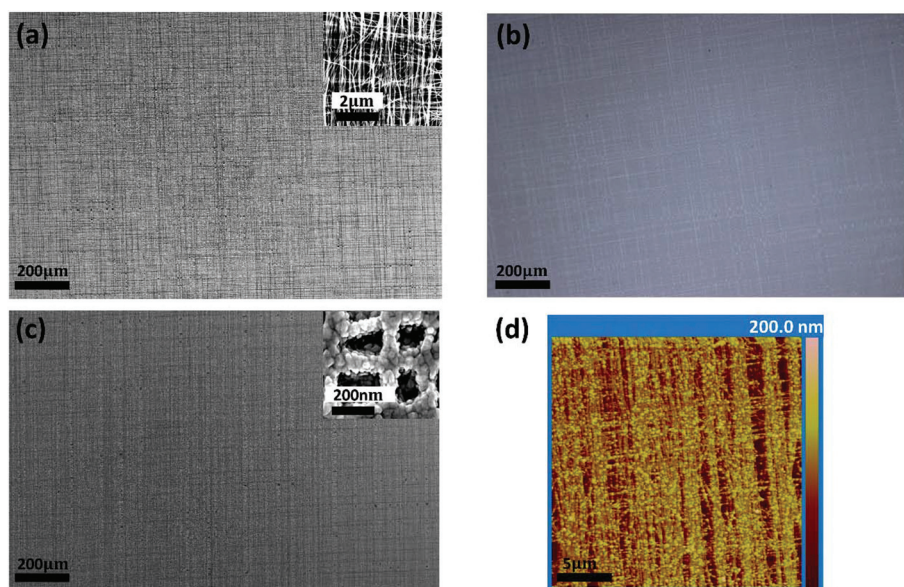


Fig. 2 (a) SEM image of the deposited SACNT networks on PET coated with a 500 nm layer of SiO_2 . The inset is the image with higher magnification. (b) Optical microscopy image of the cross-nanoporous structures of SiO_2 on PET. (c) Representative SEM image of the cross-nanoporous structures of gold with distinctive features of the SACNT grid. The inset shows a high-resolution image of the sample. (d) AFM image of the flexible SERS-active substrate, showing the presence of gold nanoparticles on the nanostructure array.

range of approximately 200–250 nm. These parameters ensured a relatively high etching rate and greater roughness of the SiO₂ grid, which is beneficial for the generation of nanogaps and sharp edges in the subsequent metal deposition.

Fig. 2(c) shows an SEM image of cross-nanoporous arrays after the deposition of a 10 nm Au layer, making it an active SERS substrate with the distinctive features of a SACNT grid, which we termed CNS of Au@PET. A Au layer thickness of 10 nm was chosen because it could lead to the formation of gold nanoparticles around the surface of the cross-nanoporous SiO₂, which helped to sustain sufficient SERS signal enhancement introduced by the generation of “hot” sites, while maintaining good flexibility and transparency. We can see that the CNS of Au are uniform over a large area and capable of ensuring good reproducibility of SERS signal enhancement. As the AFM image in Fig. 2(d) and a high resolution image of the sample shown in the inset in Fig. 2(c) demonstrate, large numbers of gold nanoparticles were created on or in the SiO₂ grid with nanogaps and sharp edges, and the overall morphology was consistent with that of SACNT networks, wherein the localized surface plasmon (LSP) and strong field enhancement would be excited by an incident electromagnetic (EM) field. For better comparison, AFM and SEM images of 10 nm unpatterned gold on the PET film are also characterized, as shown in Fig. S2(b) and (c).[†] Furthermore, this scheme leads to complex nanosystems, particularly the “Au NPs@SiO₂ nano-

wire” multidimensional structure and “Au NPs–Au NPs” adjacent cells, which may further enhance the localized EM field by efficient coupling of various LSPs.

The proposed method has exhibited some distinct advantages of the production of flexible and transparent SERS-active substrates. CNS of SiO₂ grids surrounded by Au nanoparticles could be readily fabricated by the combination of SiO₂ etching and Au layer deposition because of the introduction of quasi-periodic SACNT networks as etching masks. As a result, the most pronounced features of the nano-scale networks were acquired with good uniformity, resulting in high reproducibility of the SERS substrate. A large number of nanogaps and sharp edges were created on the surface or side walls of the crossed SiO₂ nanowires, which could greatly improve the detection sensitivity by the excitation of dense “hot spots”. This occurred primarily because the streaks and verticality of structures were largely affected by the detailed shape and etching selectivity of the Al₂O₃-coated SACNT mask, and the choice of the Au layer critical thickness. A relatively high transparency flexible SERS substrate would be obtained using the above fabrication process and parameters, as shown in the photograph in Fig. 3(a). For comparison, the photograph of a pure PET film is also shown in Fig. 3(b). In addition, the as-fabricated CNS of Au@PET could be produced with a large area using this method owing to the availability of large-scale SACNT networks. Fig. 3(a) shows a representative flexible SERS-active sub-

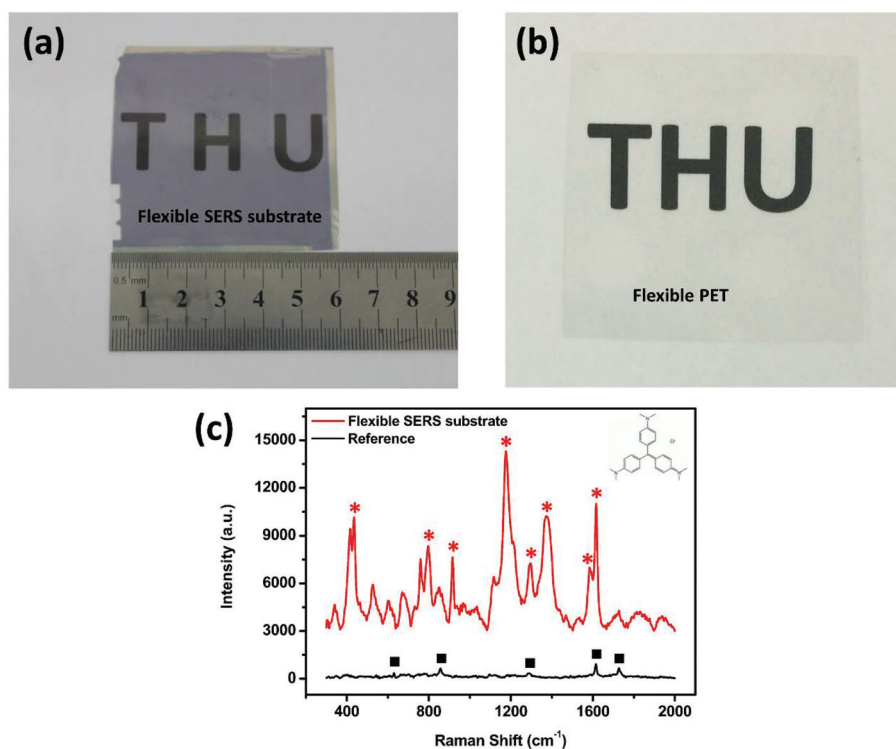


Fig. 3 Photograph of (a) the as-fabricated flexible SERS substrate with good transparency at a scale of 60 × 60 mm, (b) the pure PET film, placed on paper printed with the letters THU (Tsinghua University). (c) Typical Raman spectra of 10⁻⁶ M crystal violet (CV) obtained from the flexible SERS-active substrate and the unpatterned gold film on PET (reference), with an exposure time of 5 s. The red asterisks and black cubes in (c) correspond to the Raman vibration modes of CV and PET, respectively.

strate that is 36 cm^2 . As SACNT arrays have been produced using batch growth, a flexible SERS substrate with an even larger area could be conveniently put into mass production in a reproducible and cost-effective manner.

As an evaluation of the sensitivity of the flexible substrates, fabricated using the method described, in SERS detection applications, CV, a common food contaminant used for food coloring and as a food additive, was selected as the probe analyte. Food is an essential element for human life, and human health would be under threat if significant food sources were polluted. Widespread attention has therefore been paid to the detection and identification of food contaminants in daily life. SERS is regarded as a reliable potential tool owing to its sensitivity in trace analysis of chemical and biological molecules. In this experiment, ten microliters of CV in ethanol with a concentration of 10^{-6} M were dropped onto the CNS of Au@PET films (detailed methods are described in the Experimental section). The SERS spectrum of CV was measured in the range $300\text{--}2000 \text{ cm}^{-1}$, after the evaporation of ethanol, with an exposure time of 5 s. For comparison, the Raman spectrum of CV molecules on PET coated with a 10 nm unpatterned gold film was also obtained as the reference, using the same settings. As shown in Fig. 3(c), high intensity Raman scattering signals of CV molecules can be clearly observed from the as-fabricated flexible SERS substrate, and the peaks are all consistent with the “fingerprint” spectrum of CV as a whole. Some characteristic vibrational modes of CV are labeled with a red asterisk. In contrast, few Raman peaks attributed to CV are observed in the reference spectrum. Instead, the pure Au-deposited PET film gave rise to several dominant Raman peaks of PET, labeled in Fig. 3(c) with black cubes. More details of the positions and assignments of the characteristic Raman bands of CV and PET are listed in Table S1 of the ESI.† It should be noted that high SERS signal enhancement can be primarily attributed to the generation of “hot spots” on the metallic nanostructures, where localized surface plasmon resonances are excited by incident light, which has been reported in numerous studies.^{7,19} The experimental results demonstrated that greatly enhanced electromagnetic fields were induced for our flexible SERS-active substrate, verifying the formation of a large number of metal nanogaps and sharp edges around the cross-nanoporous SiO_2 . This was also demonstrated by the finite difference time domain (FDTD) simulations of the CNS of Au with a simplified ideal model in front-side mode, which is shown in Fig. S3(a) and (b) of the ESI.† The spatial intensity distribution of the local electromagnetic field near the nanostructures shows a high density of “hot spots” from nanogaps and sharp edges, where the markedly large enhancement depicted by a factor of $\left(\frac{E}{E_0}\right)^2$ can reach 3.4×10^3 , appearing on the top surface of the structures. For comparison, the simulated intensity distribution of the local electromagnetic field of 10 nm Au@PET is also shown in Fig. S2(d),† with a maximal EM field enhancement factor of ~ 2.5 .

We carried out UV-vis transmission spectroscopy measurements to reveal the optical properties of the resulting SERS substrates. It is important for support materials of SERS-active substrates to have good flexibility and transparency in real-time for on-site SERS applications. As Fig. 4(a) shows, the pure PET film and the cross-nanoporous SiO_2 have a transmittance of $\sim 90\%$, ensuring that the incident laser can easily pass through the PET film and access the gold nanoparticles formed around the CNS of SiO_2 . Localized surface plasmons of the formed Au nanoparticles would be stimulated and then a very strong local electromagnetic field, with a homogeneous distribution, could be formed widely around the nanogaps between the metal NPs and sharp edges. As a result, it is anticipated that the Raman signals of probe molecules adsorbed on the CNS of Au would be significantly amplified. A transmission valley with a broad band at $\sim 630 \text{ nm}$ from the resultant substrate is shown as a green curve in Fig. 4(a), and could be considered to be the absorption band due to the excitation of LSPR of the CNS of Au. This would indicate the formation of Au nanostructures around the SiO_2 grid of the substrate, and mean that abundant SERS “hot spots” in the nanogaps and sharp edges would be excited by irradiation with a laser with a wavelength of $\sim 630 \text{ nm}$. For comparison, the transmission of PET coated with a 10 nm Au layer was also plotted, shown by the blue spectrum.

A sensitivity study was performed on the resulting flexible substrate to evaluate the feasibility of on-site SERS analysis. Concise models of Au NPs around cross-nanoporous SiO_2 were constructed according to our observations, for illustrating different measurement modes (front-side mode and back-side mode), as shown in Fig. 4(b) and (c), wherein SERS signals were collected from both sides of the “CNS of Au@PET”, after exposure to the incident laser. A set of experiments for SERS detection of CV solutions with concentrations from 10^{-6} to 10^{-9} M were conducted on the resulting flexible SERS substrates (detailed methods are given in the Experimental section). Fig. 4(d) shows the normalized SERS spectrum of CV measured in both modes with an exposure time of 5 s. For comparison, the background SERS spectra of bare CNS of Au@PET without CV molecules are also shown in Fig. 4d, and denoted as blank. It can be seen that the intensities of peaks obtained from both sides of the substrate were almost the same. And interestingly, the signals collected in back-side mode were even stronger, which supported the above anticipation that the Raman signals of probe molecules adsorbed on the CNS of Au would be largely enhanced by exciting the LSP of Au nanoparticles formed on the reverse of the substrate, in back-side mode. To further validate the anticipation and investigate the mechanism of the experimental results, FDTD simulations were carried out under the perpendicular irradiation of a laser with a wavelength of 632.8 nm , in the back-side mode as shown in Fig. S3(c) of the ESI.† It is clear that the total EM field can also be significantly enhanced by a high density of “hot spots” generated from nanogaps and sharp edges, as shown in Fig. S3(d),† where the maximal EM field enhancement factor can reach 1.6×10^4 , which appears

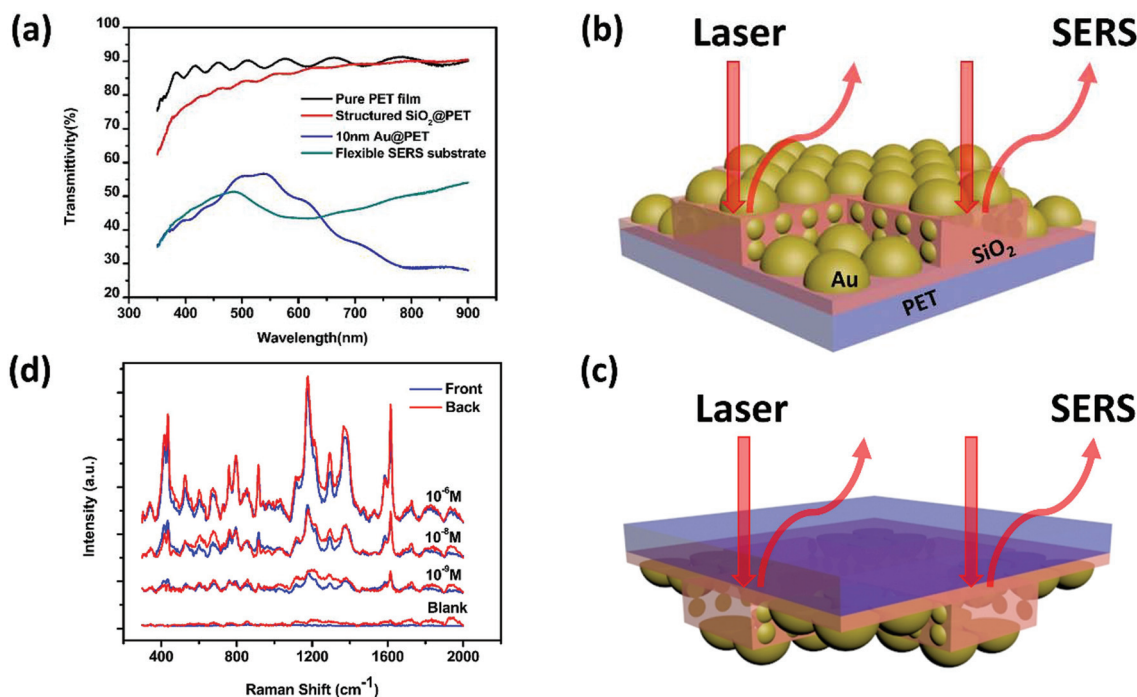


Fig. 4 (a) UV-vis transmission spectrum of a pure PET film, the cross-nanoporous structure of SiO₂ on PET, 10 nm gold films on PET, and a flexible PET-based SERS substrate. Schematic diagram of SERS experiment, in which the flexible SERS-active substrate is irradiated with a laser beam from the (b) front side and (c) back side. (d) SERS spectra of CV, obtained from both sides of the flexible and transparent SERS substrate, with analyte concentrations of 10⁻⁶, 10⁻⁸ and 10⁻⁹ M dropped onto its surface. The exposure time was 5 s.

in the grooves of the CNS of Au and is about 4 times stronger than that for the front-side mode. This phenomenon occurs because the LSPR of noble metal nanoparticles or sharp edges is dominated by the dipole mode and then significantly related to the surrounding dielectric constant. Under the back-side irradiation and measurement, the surrounding medium can be regarded as SiO₂, in which the dielectric constant would be well matched with the complex dielectric function of the metal. A stronger resonance occurs in this situation compared with that for the front-side mode, where the surrounding medium is air.

Experimental results of Fig. 4(d) also showed that a small minority of weak Raman signals from the PET film could be detected from the flexible SERS substrate in back-side mode measurement, on account of the small spacing between the PET film and the CNS of Au, for example the band at ~1720 cm⁻¹. However, this had no impact on the analysis of the probe molecules because the Raman spectra can be regarded as “fingerprints” for various chemical and biological substances. In addition, the detection limit of CV in ethanol, in which the analytes were dropped onto the flexible substrate, was found to be as low as 0.1 nM. We therefore expect that the CNS of Au@PET could adsorb on irregular objects and collect signals in back-side mode without the attenuation of the intensity, which has significant potential in real-time and on-site SERS analysis.

The flexibility of the as-fabricated SERS substrates was also evaluated and characterized by bending them for five cycles at

a radius of less than 3 mm and after that detecting their SERS activity, as shown in Fig. S4 in the ESI,[†] from which we can conclude that the flexible substrate could endure an appropriate bending strain and sustain the high activity of SERS performance. These results demonstrate that the flexible SERS substrate has good mechanical properties, and the mechanical bending has little effect on the excitation of “hot spots” from narrow metal nanogaps and sharp edges. Thus the as-fabricated substrate is suitable for the application of flexible SERS sensing.

On the basis of the results discussed, it is clear that the CNS of Au@PET is a promising SERS substrate for rapid, on-site SERS detection. A small piece of the resultant SERS-active substrate was applied to the surface of a tomato and was able to make good contact due to its flexibility, as can be seen in the photograph in Fig. 5(a). The inset demonstrates the flexibility of the sensing substrate through bending at a radius of less than 3 mm. Relatively high transparency and flexibility of the support materials, as well as cost-effective preparation and excellent SERS performance, mean that the versatile substrates can be used for identifying biochemical analytes on the surface of irregular objects, through a simple “adsorbing or wrapping” method with the CNS of Au@PET film and stimulating the localized surface plasmons of the Au nanostructures by the incident EM field penetrating the PET film. For proof of this concept, real-time on-site SERS detection of the CV molecules on the tomato surface, using the flexible substrate, was demonstrated according to the specific sample preparation

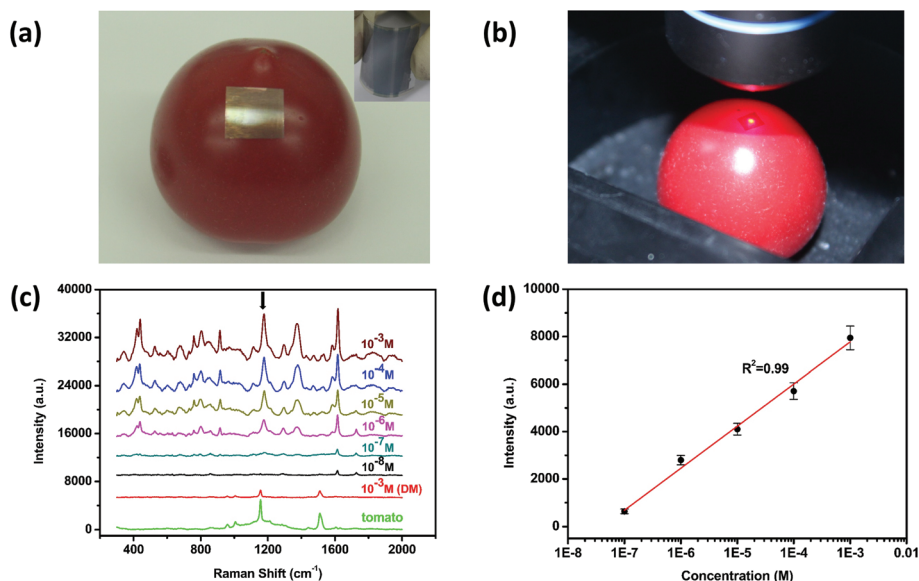


Fig. 5 Performance test of the flexible SERS-active substrate. (a) Photograph showing the as-fabricated flexible substrate being applied to the tomato surface. The inset depicts the excellent mechanical flexibility of the substrate with bending. (b) Real-time and on-site SERS detection of CV sprayed onto an irregular tomato surface using the flexible substrate. (c) SERS spectra of CV obtained from the back-side of the flexible substrate, with different concentrations ranging from 10⁻³ to 10⁻⁸ M sprayed on the tomato surface. The direct measurement (DM) of the Raman spectra of CV (10⁻³ M) on the tomato surface and the Raman spectra of the tomato are shown in the red and green curves, respectively. (d) Linear variation in the SERS intensity of CV at 1174 cm⁻¹ labeled in (c) versus logarithmic CV concentration. The exposure time was 5 s.

described in the Experimental section, as shown in Fig. 5(b). SERS signals were directly recorded in back-side mode by focusing the laser spot onto the interface between the flexible substrate and the tomato surface. As Fig. 5(c) shows, no distinct CV Raman signals could be detected by direct measurement (DM) of the tomato after spraying with a CV solution with a concentration of 10⁻³ M. The spectrum included several peaks assigned to carotenoid from the tomato, including the bands at 1157 cm⁻¹ and 1510 cm⁻¹. The Raman spectrum of pure tomato without CV adsorption was also measured as a reference. By comparison, significant Raman signal enhancement associated with CV was observed when the flexible CNS of Au@PET was adsorbed on the surface of the tomato. This significant enhancement is attributed to the contact between the active side of the substrate and the residual CV on the tomato. Because of the extremely low concentration of residual food contaminants in daily life, it is necessary to establish the sensitivity of the resultant flexible substrate in an analytical application. The SERS spectra of CV, with a series of molecule concentrations ranging from 10⁻³ M to 10⁻⁸ M, were obtained using consistent measurement conditions. With this approach, the on-site SERS intensity could still be detected when a CV concentration as low as 10⁻⁷ M remained on the tomato. In the experiment, the tomato surface was sprayed with a CV solution with a particular concentration. According to the experiment, it is estimated that the amount of CV ethanol solution on one spot is about 20 μL during the spraying, which covers an area of the circle with ~0.3 cm radius. Thus the limit of detection of CV on the tomato surface is about 2.9 ng cm⁻².

More importantly, no contaminants were introduced to the sampled object during the fast detection.

Additionally, it could be seen that the original SERS intensity of the CV spectrum clearly decreased as the CV concentration was reduced from 10⁻³ M to 10⁻⁷ M. The intensity of the Raman band at 1174 cm⁻¹, corresponding to the in-plane vibration of the ring C–H bend in the CV molecule, as a function of CV concentration, is shown in Fig. 5(d). It can be seen that the relationship between the intensity of the Raman band at 1174 cm⁻¹ and the logarithm of the CV concentration, is linear, with an R² of 0.99. In light of these experimental results, we can make a preliminary analysis of the unknown concentration of residual CV molecules on objects, by measuring the SERS intensity. As a result, it is believed that the flexible SERS substrates are promising for quantitative detection of contaminant residues on irregular objects, and could be extended to other practical applications.

The ability to efficiently extract trace amounts of analyte from irregular surfaces in routine applications is regarded as one of the prominent advantages of the flexible SERS-active substrate. We therefore further demonstrated the versatility of the as-fabricated flexible CNS of Au@PET film in SERS detection by swabbing the skin of an apple sprayed with traces of 4-ATP, a chemical used as a pesticide, medicine and dye-intermediate. The detailed sample preparation can be found in the Experimental section. Because of its flexibility, the wetted SERS-active substrate could achieve close contact with the apple skin through mechanical swabbing, shown in the inset of Fig. 6(a), thus resulting in the efficient extraction of the

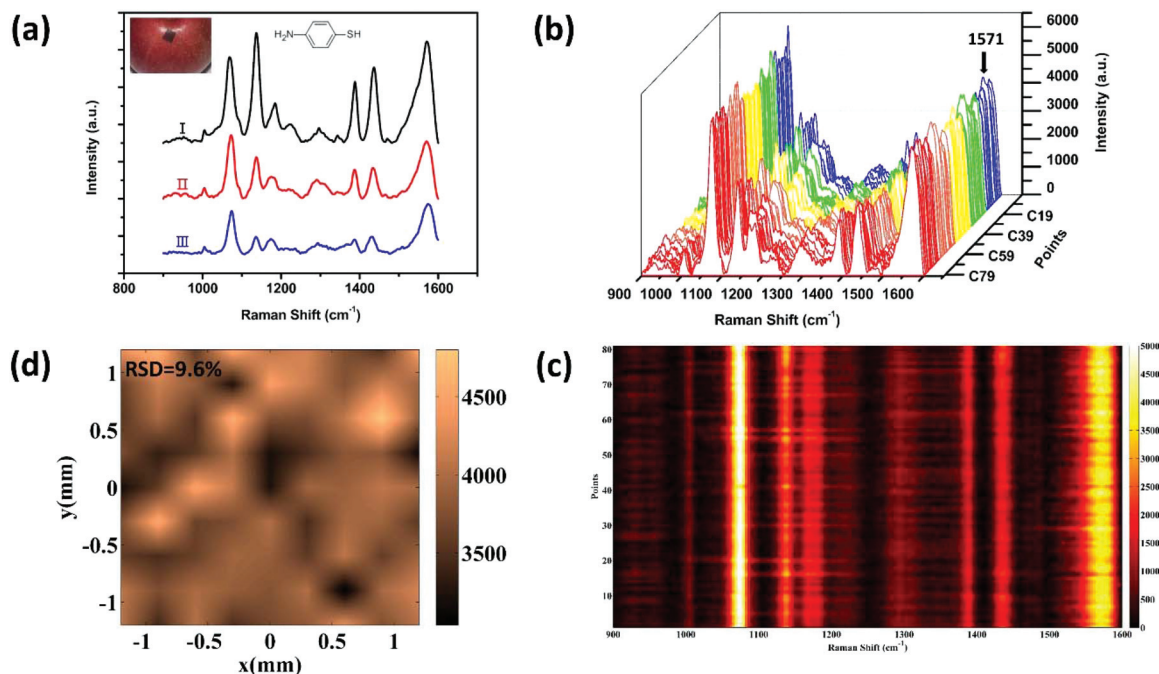


Fig. 6 (a) SERS spectra of 4-ATP obtained from the resultant flexible substrate: (I), (II) after being immersed in 4-ATP solutions with concentrations of 10^{-6} M (black curve) and 10^{-8} M (red curve); (III) after swabbing the apple skin sprayed with 10^{-6} M 4-ATP solution, shown in the upper-left inset. (b), (c) SERS waterfall plots and contour map of 10^{-6} M 4-ATP obtained from 81 spots with a step width of $300\ \mu\text{m}$ on the flexible SERS-active substrate. (d) Raman intensity distribution plot of 10^{-6} M 4-ATP at the major peak of 1571 cm^{-1} with a $2.5 \times 2.5\text{ mm}$ area and a relative standard deviation (RSD) of 9.6%. Experimental conditions: Exposure time of 30 s for (a) and 20 s for (b)–(d).

residual 4-ATP molecules. Subsequently, the SERS analysis was conducted on the active side of the flexible substrate. The Raman spectrum obtained from the substrate after swabbing the apple skin sprayed with 10^{-6} M 4-ATP solution, is indicated in spectrum III of Fig. 6(a). For comparison, spectra I and II are the SERS spectra of 4-ATP obtained from two flexible substrates after being soaked in 4-ATP solution with a concentration of 10^{-6} M and 10^{-8} M, respectively. All of the Raman peaks are in good agreement with the characteristic bands of 4-ATP, whose peak positions and assignments are partly listed in Table S2 of the ESI.† Moreover, the thiram pesticides with relatively weak affinity to the Au surface, which have been applied to the tomato, were selected to perform similar detections using the swabbing method. The detailed SERS spectra are shown in Fig. S5 of the ESI,† in which several representative peaks are labelled and are consistent with the spectrum assigned to the thiram. Similarly, the Raman intensity obtained from the substrate after swabbing the apple skin applied with 10^{-5} M thiram solution, was largely enhanced, as shown in spectrum III of Fig. S5.† For comparison, spectra I and II are the SERS spectra of thiram measured from two flexible substrates after being immersed in thiram ethanol solutions with concentrations of 10^{-5} M (black curve) and 10^{-7} M (red curve) for 1 h. The results revealed that the Raman intensity could be greatly enhanced by using the swabbing technique, verifying that the proposed flexible substrate has the potential to be applied to the efficient extraction of analytes and fast SERS detection.

Uniformity is considered an important feature of flexible SERS-active substrates. We therefore investigated the reproducibility of the detection of 4-ATP molecules using the resultant CNS of Au@PET substrate. After soaking the flexible substrate in a 10^{-6} M 4-ATP solution, SERS spectra were recorded from 81 spots with a step width of $300\ \mu\text{m}$ along two orthogonal directions, depicted as waterfall plots, shown in Fig. 6(b). Fig. 6(c) shows the corresponding contour map of all Raman peaks assigned to 4-ATP, such as the characteristic bands at 1073 , 1138 , 1388 , 1435 and 157 cm^{-1} . This demonstrates that all SERS signals were strongly enhanced with good uniformity, revealing the high performance of the flexible substrate on a large-scale area. The high reproducibility of the flexible substrate could be attributed to the high density “hot spots” of the cross-nanoporous structures of Au. Moreover, the relative standard deviation (RSD) of the SERS intensity of the peak at 1571 cm^{-1} is 9.6%, as shown in Fig. 6(d), which describes the intensity distribution plot as a function of position throughout the SERS substrate with an area of $2.5 \times 2.5\text{ mm}$. The RSDs of the intensity of other vibrational bands at 1073 , 1138 , 1388 and 1435 cm^{-1} were also calculated, shown in Fig. S6 of the ESI.† The comparatively low RSD further indicated the high uniformity of the proposed flexible SERS-active substrate.

Conclusions

In summary, a flexible and transparent CNS of Au@PET film was fabricated as a versatile and effective SERS substrate *via* a

cost-effective strategy based on etching and metal evaporation. It was observed that a large number of metal nanogaps and sharp edges around the cross-nanoporous SiO₂ were established in the resulting substrate, leading to abundant “hot spots” with good uniformity. The high SERS enhancement effect of the proposed flexible SERS-active substrate was demonstrated using CV as an analyte, in both front-side and back-side measurement modes. Specifically, the flexible substrates allow for fast, on-site and ultrasensitive SERS detection of food contaminants, by wrapping the irregular surfaces of fruits, with a lowest CV solution concentration detected on tomato skin down to 10⁻⁷ M. A preliminary quantitative analysis of contaminant residues could be performed based on the experimental linear relationship between the intensity of the Raman band at 1174 cm⁻¹ and the logarithmic CV concentration in routine applications. In addition, the detection of 10⁻⁶ M 4-ATP and 10⁻⁵ M thiram was achieved by swabbing apple skin with the CNS of Au@PET film owing to its ability to efficiently extract trace amounts of analyte from objects. It was also shown that the resultant flexible SERS substrate with cross-nanoporous structures possessed excellent detection reproducibility, with an RSD value of the major Raman band of less than 10% over a large-scale area. It is clear that these results demonstrate that the flexible substrate fabricated using this approach could potentially be used as a real-time, fast, on-site SERS platform in food safety and environmental monitoring.

Experimental section

Materials

Polyethylene terephthalate (PET) films with a thickness of 75 μm were purchased from PANAC. Crystal Violet (CV) was purchased from Alfa Aesar. 4-Aminothiophenol (4-ATP) and thiram were purchased from Sigma-Aldrich. Good quality super-aligned CNT arrays with a height of 300 μm were synthesized on 8-inch silicon wafers by low-pressure chemical vapor deposition (LP-CVD), which is described in previous work.⁴³

Transfer of super-aligned CNTs

Prior to the deposition of SiO₂, the PET film was heated on a hotplate for 20 min (100 °C) to induce the release of stress, preventing thermal strain in the subsequent etching process and metal deposition. The suspended SACNT networks cross-stacked on the metal frame were placed on the ready-made SiO₂/PET substrate. Several drops of alcohol were added to the surface of the SACNT, which caused the CNTs to shrink, making the CNTs bind with the SiO₂-coated PET substrate more compactly.

Preparation of SERS detection samples

To demonstrate the SERS sensitivity, including being excited from both the front and back sides, CV in ethanol solution (bulk concentration of 10⁻³ M) was prepared as a stock solu-

tion, and different concentrations (10⁻⁶ M, 10⁻⁸ M and 10⁻⁹ M) of CV ethanol solution were obtained by dilution of the stock solution. Then 10 μL of the different diluted solutions was dropped onto the flexible SERS substrates and dried in air at room temperature. To explore the versatility of the as-fabricated CNS of Au@PET as a flexible SERS substrate for real-time and on-site molecule detection, a small piece of substrate with the active side down was adsorbed onto the surfaces of tomatoes, to which different concentrations of CV ethanol solution, ranging from 10⁻³ M to 10⁻⁸ M, had been applied. The samples were subsequently dried at room temperature. The SERS signals were directly measured from the reverse side of the substrates. A direct measurement was also carried out by focusing the incident laser onto the tomato surface in the absence of the sensing substrate. An apple to which a 4-ATP ethanol solution with a concentration of 10⁻⁶ M had been applied, was measured in the same manner. The flexible SERS-active films, slightly wetted by adding a small drop of ethanol, were used to mechanically swab the skin of the prepared apple three times, and the SERS spectra were obtained from the active side of the flexible substrate. For comparison, two equivalent flexible substrates were soaked in 4-ATP solution with concentrations of 10⁻⁶ M and 10⁻⁸ M for 4 h and characterized as previously described.

Characterization

Nanostructures of the resultant flexible SERS substrates were characterized using SEM and AFM. SEM images were obtained using an FEI Nova NanoSEM 450. AFM images were taken using an NT-MDT AFM in tapping mode. Microscopy images were acquired at 100× optical magnification. UV-vis transmission spectra were recorded with a lambda 950 spectrometer in the range 350–900 nm. The SERS measurements were performed in backscattering mode using a confocal micro-Raman spectrometer (Jobin-Yvon LabRam HR800) with a laser excitation wavelength of 632.8 nm at room temperature. A BH-2 microscope with 50× objective lens (nominal numerical aperture; 0.75) and a Peltier cooled charge coupled device (CCD) were used for all Raman signal collection. The laser spot size for signal probing was ~2 μm in diameter, and the incident excitation power was set at 1.7 mW with different exposure times. All Raman spectra were fitted using the Gaussian-Lorentzian lineshape after the removal of the baseline.

Conflicts of interest

There are no conflicts to declare.

Acknowledgements

This work was financially supported by the National Natural Science Foundation of China (11574171, 51532008), the National Key Research and Development Program of China

(2017YFA0205800) and the China Postdoctoral Science Foundation (2016M601012).

Notes and references

- 1 M. Fleischmann, P. J. Hendra and A. J. McQuillan, *Chem. Phys. Lett.*, 1974, **26**, 163–166.
- 2 M. Moskovits, *Rev. Mod. Phys.*, 1985, **57**, 783.
- 3 L. Qu, Y. Liu, S. He, J. Chen, Y. Liang and H. Li, *Biosens. Bioelectron.*, 2016, **77**, 292–298.
- 4 Z. Liu, Z. Yang, B. Peng, C. Cao, C. Zhang, H. You, Q. Xiong, Z. Li and J. Fang, *Adv. Mater.*, 2014, **26**, 2431–2439.
- 5 L. Zhang, T. Liu, K. Liu, L. Han, Y. Yin and C. Gao, *Nano Lett.*, 2015, **15**, 4448–4454.
- 6 S. Nie and S. R. Emory, *Science*, 1997, **275**, 1102–1106.
- 7 M. S. Schmidt, J. Hübner and A. Boisen, *Adv. Mater.*, 2012, **24**, 11–18.
- 8 K. Kneipp, Y. Wang, H. Kneipp, L. T. Perelman, I. Itzkan, R. R. Dasari and M. S. Feld, *Phys. Rev. Lett.*, 1977, **78**, 1667.
- 9 S. L. Kleinman, E. Ringe, N. Valley, K. L. Wustholz, E. Phillips, K. A. Scheidt, G. C. Schatz and R. P. Van Duyne, *J. Am. Chem. Soc.*, 2011, **133**, 4115–4122.
- 10 D. Li, L. Qu, W. Zhai, J. Xue, J. S. Fossey and Y. Long, *Environ. Sci. Technol.*, 2011, **45**, 4046–4052.
- 11 Z. Gong, H. Du, F. Cheng, C. Wang, C. Wang and M. Fan, *ACS Appl. Mater. Interfaces*, 2014, **6**, 21931–21937.
- 12 J. Li, Y. Huang, Y. Ding, Z. Yang, S. Li, X. Zhou, F. Fan, W. Zhang, Z. Zhou, D. Wu, B. Ren, Z. Wang and Z. Tian, *Nature*, 2010, **464**, 392.
- 13 G. Bodelón, V. Montes-García, V. López-Puente, E. H. Hill, C. Hamon, M. N. Sanz-Ortiz, S. Rodal-Cedeiram, C. Costas, S. Celiksoy, I. Pérez-Juste, L. Scarabelli, A. L. Porta, J. Pérez-Juste and I. Pastoriza-Santos, *Nat. Mater.*, 2016, **15**, 1203–1211.
- 14 J. Ando, K. Fujita, N. I. Smith and S. Kawata, *Nano Lett.*, 2011, **11**, 5344–5348.
- 15 A. Champion, J. E. Ivanecky III, C. M. Child and M. Foster, *J. Am. Chem. Soc.*, 1995, **117**, 11807–11808.
- 16 L. Jensen, C. M. Aikens and G. C. Schatz, *Chem. Soc. Rev.*, 2008, **37**, 1061–1073.
- 17 H. Ko, S. Singamaneni and V. V. Tsukruk, *Small*, 2008, **4**, 1576–1599.
- 18 K. Liu, Y. Bai, L. Zhang, Z. Yang, Q. Fan, H. Zheng, Y. Yin and C. Gao, *Nano Lett.*, 2016, **16**, 3675–3681.
- 19 Y. J. Oh and K. H. Jeong, *Adv. Mater.*, 2012, **24**, 2234–2237.
- 20 M. Hu, F. S. Ou, W. Wu, I. Naumov, X. Li, A. M. Bratkovsky, R. S. Williams and Z. Li, *J. Am. Chem. Soc.*, 2010, **132**, 12820–12822.
- 21 J. Yang, M. Palla, F. G. Bosco, T. Rindzevicius, T. S. Alstrøm, M. S. Schmidt, A. Boisen, J. Ju and Q. Lin, *ACS Nano*, 2013, **7**, 5350–5359.
- 22 D. K. Lim, K. S. Jeon, J. H. Hwang, H. Kim, S. Kwon, Y. D. Suh and J. M. Nam, *Nat. Nanotechnol.*, 2011, **6**, 452–460.
- 23 M. E. Stewart, M. J. Motala, J. Yao, L. B. Thompson and R. G. Nuzzo, *Proc. Inst. Mech. Eng., Part N*, 2007, **220**, 81–138.
- 24 N. A. Abu Hatab, J. M. Oran and M. J. Sepaniak, *ACS Nano*, 2008, **2**, 377–385.
- 25 Z. Zhu, B. Bai, H. Duan, H. Zhang, M. Zhang, O. You, Q. Li, Q. Tan, J. Wang, S. Fan and G. Jin, *Small*, 2014, **10**, 1603–1611.
- 26 K. N. Kanipe, P. P. Chidester, G. D. Stucky and M. Moskovits, *ACS Nano*, 2016, **10**, 7566–7571.
- 27 R. Liu, S. Li and J. F. Liu, *TrAC, Trends Anal. Chem.*, 2017, **97**, 188–200.
- 28 Y. Ma and L. Y. L. Yung, *ACS Appl. Mater. Interfaces*, 2016, **8**, 15567–15573.
- 29 L. Polavarapu and L. M. Liz-Marzán, *Chem. Phys.*, 2013, **15**, 5288–5300.
- 30 A. Martín, J. J. Wang and D. Iacopino, *RSC Adv.*, 2014, **4**, 20038–20043.
- 31 C. H. Lee, L. Tian and S. Singamaneni, *ACS Appl. Mater. Interfaces*, 2010, **2**, 3429–3435.
- 32 M. Fan, Z. Zhang, J. Hu, F. Cheng, C. Wang, C. Tang, J. Lin, A. G. Brolo and H. Zhan, *Mater. Lett.*, 2014, **133**, 57–59.
- 33 J. Chen, Y. Huang, P. Kannan, L. Zhang, Z. Lin, J. Zhang, T. Chen and L. Guo, *Anal. Chem.*, 2016, **88**, 2149–2155.
- 34 H. Tian, N. Zhang, L. Tong and J. Zhang, *Small Methods*, 2017, **1**, 6.
- 35 G. Lu, H. Li and H. Zhang, *Small*, 2012, **8**, 1336–1340.
- 36 V. Suresh and F. L. Yap, *RSC Adv.*, 2015, **5**, 61671–61677.
- 37 Z. Li, G. Meng, Q. Huang, X. Hu, X. He, H. Tang, Z. Wang and F. Li, *Small*, 2015, **11**, 5452–5459.
- 38 W. Wu, L. Liu, Z. Dai, J. Liu, S. Yang, L. Zhou, X. Xiao, C. Jiang and V. A. Roy, *Sci. Rep.*, 2015, **5**, 10208.
- 39 S. K. Bhunia, L. Zeiri, J. Manna, S. Nandi and R. Jelinek, *ACS Appl. Mater. Interfaces*, 2016, **8**, 25637–25643.
- 40 Y. Jin, Q. Li, M. Chen, G. Li, Y. Zhao, X. Xiao, J. Wang, K. Jiang and S. Fan, *Small*, 2015, **11**, 4111–4116.
- 41 Y. Jin, Y. Wang, M. Chen, X. Xiao, T. Zhang, J. Wang, K. Jiang, S. Fan and Q. Li, *ACS Appl. Mater. Interfaces*, 2017, **9**, 32369–32376.
- 42 K. Jiang, J. Wang, Q. Li, L. Liu, C. Liu and S. Fan, *Adv. Mater.*, 2011, **23**, 1154–1161.
- 43 Y. Sun, K. Liu, J. Miao, Z. Wang, B. Tian, L. Zhang, Q. Li, S. Fan and K. Jiang, *Nano Lett.*, 2010, **10**, 1747–1753.